

# OPTICAL SPECTROSCOPY OF A QUANTUM CARBON WIRE

Peter C. Eklund<sup>1</sup>

Center for Applied Energy Research and  
Department of Physics and Astronomy  
University of Kentucky, Lexington, KY 40506

Keywords: carbon nanotubes, Raman scattering, quantum confinement

**Abstract** Raman Spectroscopy has been used to probe the vibrational modes of carbon nanotubes. The Raman spectrum of this new form of carbon is very different from that observed for graphite (the nanotube's flat parent) and these differences can be understood as a result of the cyclic boundary condition imposed on a graphene sheet rolled up to form a seamless nanotube. Optical resonances are observed which are associated with the one dimensional character of the electronic states of these novel quantum wires.

## INTRODUCTION

Single wall nanotubes (SWNTs) were discovered in 1993 in the carbonaceous by-products from an arc discharge between carbon electrodes in an inert atmosphere [2,3]. They have been observed directly in electron microscopes and in scanning tunneling microscopes. In this paper, we wish to explore the special nature of these one dimensional (1D) carbon quantum wires using Raman spectroscopy. The quantum effects we observe here cannot be observed in the so-called "multiwall carbon nanotubes" (MWNTs) which were discovered a few years earlier also in the soot from a carbon arc[4]. These MWNTs are comprised of a series of concentric SWNTs with an inter-shell spacing of about 3.4 Å. The inner diameter of the MWNT is typically 5-10 times larger than a SWNT. As small as these diameters are in terms of a micron scale, they are too large to observe the quantum size effects we observe in SWNTs with diameters ~ 1nm.

In Fig. 1 the  $sp^2$  based structure of a seamless carbon nanotube is shown schematically. The hexagonal arrangement of C-atoms, identical to that in flat carbon sheets of graphite, are apparent in the figure. Three different subclasses of seamless nanotubes can be formed: armchair (n, n), zigzag (n, 0) and chiral (n,  $m \neq n$ ) where the integers n and m are used to define the symmetry of the nanotube [4]. Understanding how to compute (n, m) are not important to understanding the principle results discussed here. It is of interest to know only that "armchair" and "zigzag" tubes have rows of hexagons aligned parallel to the tube axis and chiral tubes can be formed such that the hexagon rows spiral up along the tube axis. The tube shown in Fig. 1 is a (9,9) armchair tube. The diameter of an armchair tube is given by  $D(\text{Å})=1.357n$ , so that a (10,10) nanotube has a diameter of 13.57 Å.

Until recently, research on the physical properties of these quantum carbon wires have been slowed by the fact that previous arc discharge methods produced mostly carbon soot and only a few % carbon nanotubes[4]. Thus experimental signals in these samples were often dominated by the response of the soot. Recently, a laser ablation technique was discovered at Rice University which produced over 70% tubes [5]. Using microfiltration, we have been able to separate the carbon nanosoot from the tubes and study reasonably pure tube samples by Raman spectroscopy. Details of the laser-assisted process developed at Rice University are available elsewhere [5]. Briefly, a carbon target containing 1-2% Ni/Co catalyst is maintained in flowing Ar in an oven (1200 °C). The carbon target is vaporized by a two-pulse sequence from a YAG and frequency-doubled YAG laser at a 10 Hz repetition rate. Nanotubes (>70%) and carbon nanospheres (~30%) and fullerenes (~1-2 %) form in the hot carbon plasma and drift downstream under flowing Ar where they are collected on a water-cooled cold finger. The carbon material was first soaked in CS<sub>2</sub> to remove solubles (i.e., fullerenes) and the insolubles were then subjected to microfiltration to physically separate the tubes and soot. This was accomplished by dispersing the material in benzalkonium chloride using ultrasound.

The resulting carbon material appears in scanning electron microscopy (SEM) images as a mat of carbon fibers. Transmission electron microscopy (TEM) was used to measure the fiber diameter. Under high resolution it was observed that the tubes were arranged into regular bundles of single-wall carbon nanotubes. These bundles, or crystalline ropes, can be seen directly in the bright field TEM image or indirectly by the electron diffraction pattern which stems from the ordered stacking of carbon cylinders. Looking at the bundle end-on, the individual tubes can be seen to organize into a two-dimensional triangular lattice. The TEM images of, and electron diffraction patterns from these crystalline ropes are shown in Figs. 2a,b. In Fig. 2c we show the size distribution determined from bright field TEM images. The mean tube diameter was also determined by x-ray diffraction (XRD). XRD and TEM yielded slightly different values for the mean tube diameter D which must stem from a non-statistical distribution of tubes selected for study in the TEM. A mean value for D consistent with a (10,10) tube was determined by XRD, in

<sup>1</sup> This paper is based, in part, on results to appear in Ref. 1.

agreement with previous XRD data on similar tubes[5]. Our bright field TEM data (Fig. 2c), however, arrived at a slightly smaller mean D value, more consistent with a (9,9) tube. As can be seen from Fig. 2c, the diameter distribution for the tubes is consistent with armchair symmetry tubes (see the tick marks in the figure) associated with the range of n-values 8-11.

In Fig. 3, we display the Raman spectrum (300 K) for purified single wall nanotubes obtained in the backscattering geometry using 514 nm Ar laser radiation. For comparison, the calculated Raman spectrum is shown below for n=8-11 armchair tubes. The frequencies were calculated in a phenomenological force constant model using the same C-C force constants used to fit vibrational data for a flat graphene sheet [6]. Note that sections of the experimental spectrum have been scaled vertically (as indicated) to best expose the rich detail. Furthermore, the frequency scale has been expanded for the highest frequency region. The theoretical Raman intensities were calculated using a bond polarizability model by Subbaswamy and co-workers [7]. The mode assignments are summarized in Table 1 and compared with theory. Further polarized Raman studies will be necessary to confirm the symmetry assignments. It may be noticed that the some of the experimental bands are narrow and some are broad. This difference is attributed to an inhomogeneous line-broadening mechanism based on the theoretical observation that particular vibrational modes exhibit a strong tube diameter dependence, while others exhibit a rather weak dependence. Thus considering that our sample contains a distribution of tube diameters, the Raman lines can be sharp (similar to a linewidth in graphite  $\sim 6 \text{ cm}^{-1}$ ) or much broad, depending on whether or not the mode frequency is strongly diameter-dependent. The intense line seen at  $186 \text{ cm}^{-1}$  in Fig. 3 is identified with the radial breathing mode in which all C-atoms are displaced radially outward in phase and the strong lines observed near  $1600 \text{ cm}^{-1}$  are related to the intralayer vibrations in graphite which are observed at  $1582 \text{ cm}^{-1}$ . In the nanotube, the cyclic boundary conditions around the tube waist activate new Raman and IR modes that are not observable in a well-ordered flat graphene sheet or in graphite--this is the first consequence of the one-dimensional (1D) nature of the nanotube. The second, to be discussed below, is the quantum confinement of the conduction electrons which gives rise to resonant Raman scattering.

The resonant nature of the Raman scattering process is clear from Fig. 4 which shows the dramatic effect on the distribution of line intensity on the frequency (or wavelength) of the excitation laser. The data were all taken at the same temperature on the same sample. Shown in the figure are spectra taken with four different lasers at the (low) power densities indicated. A closer inspection of the figure reveals that not only are the intensities changing dramatically with laser frequency, but so are the Raman line frequencies!! The former effect is typical of resonant Raman scattering in many solid, gas and liquid samples, whereas the latter is a manifestation of a series of resonances each identified with different tube diameters (e.g., (n,n)). In general, resonantly enhanced Raman scattering occurs when the energy of the incident photon matches the transition energy of a strong optical absorption band [8]. Normally, the Raman line intensity can jump by several orders of magnitude, but the Raman line frequency is fixed or varies very slightly. In the present work, large shifts in frequency are also observed which is quite unusual.

We now provide a simple explanation for this observation based on tube-diameter-dependent optical absorptions which stem from the 1D nature of the single wall carbon nanotube. A more complete theoretical explanation will be forthcoming [7]. For large enough tube diameter, the character of the electronic states in a carbon nanotube should be essentially independent of tube diameter (or n in (n,n)) and should resemble closely that of a flat graphene sheet. These larger tubes therefore should respond to the excitation laser as does graphite, or more precisely a single graphene sheet, exhibiting no strong resonance(s) in the region of interest here and only one Raman line at  $\sim 1582 \text{ cm}^{-1}$ . This is what is observed, for example, in much larger diameter multiwall carbon nanotubes. A change in laser excitation wavelength (or frequency) is found to produce small changes in the Raman intensity and extremely small (if detectable) changes in the frequency of the  $1582 \text{ cm}^{-1}$  mode. The large shifts in Raman line frequency we observe are therefore identified with a diameter-dependent optical absorption which promotes resonant scattering from particular diameter tubes. The shifting frequency is both the result of the sample being a collection of different diameter tubes and the fact that these different diameter tubes have different optical resonances. In 1D systems it is well known that  $E^{-1/2}$  singularities exist in the electronic density of states (DOS). These singularities manifest themselves as spikes in the DOS calculated for n=8,11 armchair tubes and shown in Fig. 5; the Fermi energy ( $E_F$ ) is taken as the energy zero. The allowed optical transitions for these tubes can be shown to be between filled states in spikes below  $E_F$  ( $v_1, v_2$ ) to empty states above  $E_F$  ( $c_1, c_2$ ). As required to explain our experimental results, the energy separation between these mirror image spikes must be diameter (n) dependent consistent with the results of Fig. 4. As one can now appreciate, Raman scattering from a (n,n) tube will dominate the spectrum when the laser photon energy matches the energy difference between spikes for that (n,n) DOS. The center of gravity of each Raman band then shifts to the frequency of the (n,n) vibrational mode being resonantly driven by the laser field.

Thus, the unusual laser frequency dependence of the Raman spectra of carbon nanotubes shown in Fig. 4 is a direct consequence of 1D quantum confinement effects in carbon nanotubes. Further work is underway to more quantitatively understand the results described above.

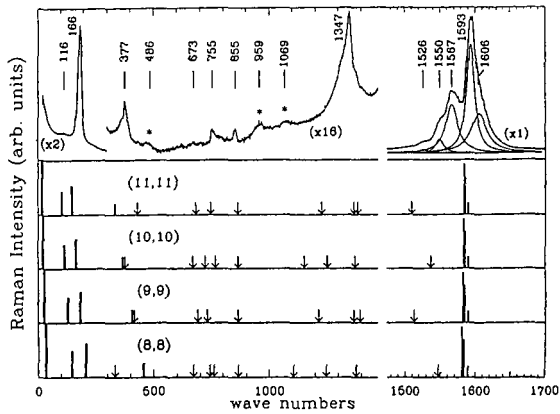


Fig. 3: Raman spectrum (top panel) of a SWNT sample taken using 514.5 nm excitation at  $\sim 2 \text{ W/cm}^2$ . The "\*" in the spectrum indicates features that are tentatively assigned to second-order Raman scattering. The four bottom panels are the calculated Raman spectra for armchair  $(n,n)$  nanotubes,  $n = 8 - 11$ . The downward-pointing arrows in the lower panels indicate the positions of the remaining weak, Raman-active modes [1].

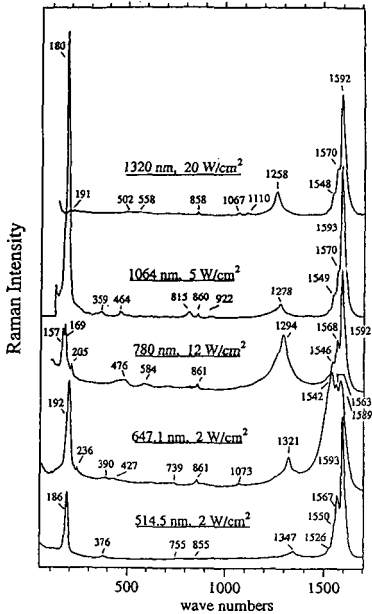


Fig. 4: Room-temperature Raman spectra for purified SWNTs, excited with five different laser frequencies. The power density for each spectrum is indicated, as are the vibrational frequencies.

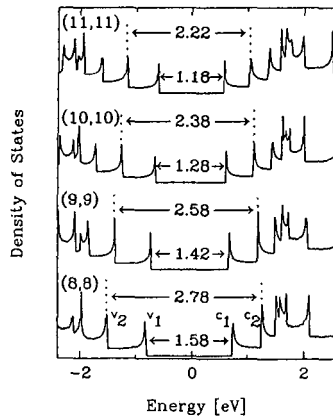


Fig. 5: Electronic density of states (DOS) calculated using a tight-binding model for  $(8,8)$ ,  $(9,9)$ ,  $(10,10)$ , and  $(11,11)$  nanotubes. The Fermi energy  $E_F$  is located at 0 eV. Wavevector-conserving optical transitions can occur between mirror-image spikes, e.g.,  $v_1 \rightarrow c_1$  and  $v_2 \rightarrow c_2$ .

## Acknowledgements

The author wishes to thank the NSF and DOE for his support during the course of this research. This paper is based on many of the results to appear in Ref. 1 and represents the fruits of a dynamic, multi-university collaboration between experimentalist and theoreticians.

## REFERENCES:

- [1] A. M. Rao, E. Richter, S. Bandow, B. Chase, P. C. Eklund, K. A. Williams, S. Fang, K. R. Subbaswamy, M. Menon, A. Thess, R. E. Smalley, G. Dresselhaus and M. S. Dresselhaus, *Science* (in press)
- [2] D. S. Bethune et al., *Nature* 363, 605 (1993).
- [3] S. Iijima and T. Ichihashi, *Nature* 363, 603 (1993).
- [4] For more details on carbon nanotubes see "*Science of Fullerenes and Carbon Nanotubes*" by M.S. Dresselhaus, G. Dresselhaus, and P. C. Eklund, Academic Press, New York, NY 1996.
- [5] A. Thess et al., *Science*, 273, 483 (1996).
- [6] R. A. Jishi et al., *Chem. Phys. Lett.*, 209, 77 (1993).
- [7] E. Richter and K. R. Subbaswamy (unpublished).
- [8] W. Hayes and R. A. Loudon, in *Light Scattering by Crystals*, (Wiley, New York, NY 1978).

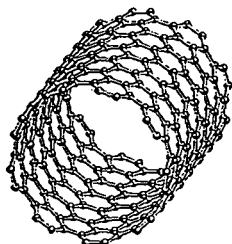


Fig. 1: Schematic model of a seamless (9,9) nanotube.

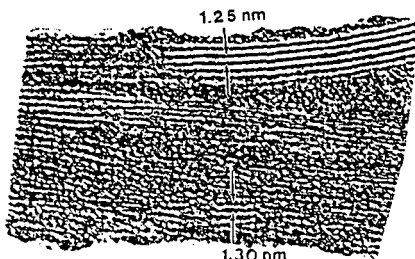


Fig. 2(a): Bright-field TEM image of a nanotube bundle. The bundles are found to be organized in triangular lattices. The arrows indicate measured approximate diameters of nanotubes within two bundles.

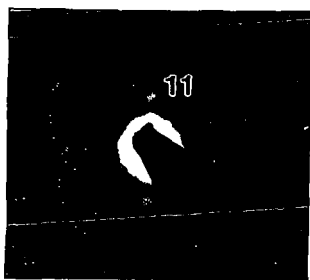


Fig. 2(b): Electron diffraction pattern with  $d_{11}$  spots corresponding to the diameter of an isolated nanotube.

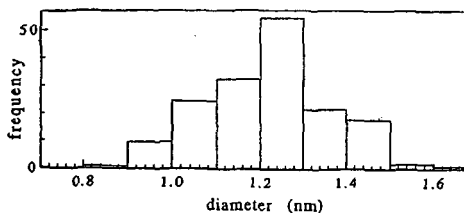


Fig. 2(c): Nanotube-diameter distribution tabulated from bright-field TEM images.

TABLES

TABLE I. First-order Raman-active vibrational mode frequencies in  $\text{cm}^{-1}$  for single-wall carbon nanotubes (SWNT): Experimental (514.5 nm excitation) and calculated. The experimental frequencies vary with laser excitation wavelength (see text and Fig. 4). The SWNT sample is thought to be an ensemble of  $n = 8 - 11$  armchair nanotubes.

Expt.		Ident. $n^b$	Sym. <sup>a</sup>	Theory <sup>c</sup>			
$\omega_0$	$I^d$			(8,8)	(9,9)	(10,10)	(11,11)
-			$E_{2g}$	34	27	22	18
116	w	10	$E_{1g}$	146	130	117	106
186	s	8,9,10	$A_{1g}$	206	183	165	150
377(s)	m	10 <sup>e</sup>	$E_{2g}$	333	-	368	-
377(b)	m	9,10 <sup>e</sup>	$E_{2g}$	458	408	371	335
-		-	$E_{1g}$		420		431
673	w	8,10	$A_{1g}$	671	-	670	-
-		-	$E_{1g}$	-	690	-	683
-		-	$E_{2g}$	-	732	-	746
-		-	$E_{2g}$	742	-	722	-
755	w	8,10	$E_{1g}$	762	-	766	-
855	w	8,9,10,11	$E_{2g}$	866	866	866	866
-		-	$E_{2g}$	1106	-	1152	-
-		-	$E_{1g}$	-	1216	-	1229
-		-	$A_{1g}$	1247	-	1252	-
1347	m	$\left\{ \begin{array}{l} 9, 11 \\ 8, 10 \end{array} \right.$	$A_{1g}$	-	1369	-	1369
			$E_{1g}$	1377	-	1374	-
1526	w	9,11	$E_{1g}$	-	1513	-	1510
1550	m	10	$E_{2g}$			1543	
1567	s	8	$E_{2g}$	1547	-	1531	-
1593	$\left. \begin{array}{l} s \\ m \end{array} \right\}$	$\left\{ \begin{array}{l} 8, 9, 10, 11 \\ 8, 9, 10, 11 \\ 8, 9, 10, 11 \end{array} \right.$	$A_{1g}$	1583	1584	1585	1586
1609			$E_{1g}$	1581	1582	1584	1585
			$E_{2g}$	1589	1589	1590	1590

<sup>a</sup>Mode symmetry as determined by model calculation.

<sup>b</sup>The  $n$  values of the armchairs nanotubes ( $n, n$ ).

<sup>c</sup>Empirical force constant model, see text.

<sup>d</sup>Intensity: w = weak, m = moderate, s = strong.

<sup>e</sup>This line at  $377 \text{ cm}^{-1}$  is a superposition of a broad (b) and a sharp (s) peak.